Chapter 9
Studies of Ferroelectric and Magnetic Phase Transitions in Multiferroic $PbFe_{0.5}B_{0.5}O_3$–$PbTiO_3$ (B = Nb, Ta) Solid Solution Ceramics

I. P. Raevski, S. P. Kubrin, A. V. Blazhevich, M. S. Molokeev, S. V. Misjul, E. V. Eremin, H. Chen, C.-C. Chou, E. I. Sitalo, S. I. Raevskaya, V. V. Titov, D. A. Sarychev, M. A. Malitskaya and I. N. Zakharchenko

Dielectric, X-ray, Mössbauer and magnetization studies of $(1-x)PbFe_{0.5}B_{0.5}O_3$–$(x)PbTiO_3$ (B = Nb, Ta) ceramics from the $0 < x < 0.3$ range have been carried out. Addition of $PbTiO_3$ to $PbFe_{0.5}B_{0.5}O_3$ increases the temperature T_m of the permittivity maximum, decreases the diffusion of this maximum and lowers the Neél temperature T_N. However above a certain compositional threshold ($x \approx 0.1$) fast lowering of T_N stops and a new magnetic state stable in a rather wide compositional range appears. Large difference between the zero-field cooled and field-cooled magnetization-temperature curves as well as between the temperatures of magnetic phase transition determined from Mössbauer and magnetization studies for compositions with $x > 0.1$ implies that this state is a spin glass phase.

I. P. Raevski · S. P. Kubrin · A. V. Blazhevich · E. I. Sitalo · S. I. Raevskaya (✉) · V. V. Titov · D. A. Sarychev · M. A. Malitskaya · I. N. Zakharchenko
Research Institute of Physics, and Physical Faculty, Southern Federal University, Rostov-on-Don, Russia
e-mail: sveta.raevskaya@mail.ru

M. S. Molokeev · E. V. Eremin
Kirensky Institute of Physics, SB RAS, Krasnoyarsk, Russia

S. V. Misjul
Siberian Federal University, Krasnoyarsk, Russia

H. Chen
University of Macau, Macau, China

C.-C. Chou
National Taiwan University of Science and Technology, Taipei, Republic of China (Taiwan)

S.-H. Chang et al. (eds.), *Advanced Materials*, Springer Proceedings in Physics 152,
DOI: 10.1007/978-3-319-03749-3_9,

9.1 Introduction

Lead iron niobate $PbFe_{0.5}Nb_{0.5}O_3$ (PFN) and lead iron tantalate $PbFe_{0.5}Ta_{0.5}O_3$ (PFT) are ternary perovskite multiferroic oxides possessing simultaneously ferroelectric and magnetic properties [1–8]. Recent burst of interest to multiferroics has the aim to find materials, which can be used to convert the magnetic signals to electric responses and *vice versa.* From this point of view, PF*B*–Pb(Zr, Ti)O_3 (B = Nb, Ta) solid solutions are among the best candidates as they were reported to possess a large magnetoelectric response at room-temperature, which is a great advantage for magnetoelectric devices [9].

At cooling, both PFN and PFT undergo the same sequence of phase transitions: from the cubic paraelectric to tetragonal ferroelectric phase at $T_{CT} \approx 380\ (270)$ K, then to the monoclinic ferroelectric phase, at $T_{TM} \approx 350$–$360\ (200$–$220)$ K, and, finally, to the G-type antiferromagnetic phase at $T_N \approx 150\ (180)$ K [1–8]. Here the data in the parenthesis correspond to PFT. Besides the AFM phase transition both PFN and PFT exhibit also the lower-temperature magnetic anomaly at $T_g \approx 10$–20 K [6, 8, 10–12]. This anomaly was at first attributed to superexchange interaction taking place via –Fe–O–Nb(Ta)–O–Fe– pathways caused by local short range chemical ordering of Fe^{3+} and $Nb^{5+}(Ta^{5+})$ ions on the nanoscale [13]. However, experiments on the temperature and magnetic field dependence of the magnetic susceptibility have shown that this anomaly marks the magnetic glass transition rather than the AFM of FM phase transition [6, 8, 10–12]. Recently a coexistence of AFM and spin glass states was approved for PFN by neutron diffuse scattering at temperatures below $\approx$20 K [12]. Studies of magnetization [2], ^{57}Fe Mossbauer spectra [14], as well as ^{93}Nb and ^{17}O NMR spectra [15] have led to the conclusion that PFN is a chemically inhomogeneous system and long range AFM order appears in Fe-rich-Nb-poor regions while, a low-temperature magnetic relaxor spin-glass state can arise from the Fe-poor-Nb-rich regions [2, 14, 15]. These data are confirmed by the results of first principles calculations showing that in PFN and PFT Fe^{3+} and Nb^{5+} (Ta^{5+}) ions are distributed in the lattice not randomly, but exhibit a sort of clustering [14]. This heterogeneity explains why the experimental values of T_N, for PFN and PFT ($\approx$150 K) are located approximately halfway between calculated values of this temperature for the fully ordered ($T_N = 0$ K) and completely disordered ($T_N \approx 300$ K) states [16].

In the present paper, we study ferroelectric and magnetic phase transition temperatures in $(1-x)$PF*B*–$(x)PbTiO_3$ solid solutions which are the cross-sections of the PF*B*–Pb(Zr, Ti)O_3 (B = Nb, Ta) system.

9.2 Experimental

PFT powder for X-ray studies was obtained by solid-state reaction route using high-purity Fe_2O_3, $PbCO_3$ and Ta_2O_5. These oxides were batched in stoichiometric proportions and mixed thoroughly together with 10 wt.% excess of $PbCO_3$ for lead

loss compensation in an agate mortar in the presence of ethyl alcohol. Then synthesis was carried out for 4 h at 850 °C. After the synthesis, the product of reaction was crushed by pestle in an agate mortar for several minutes and then annealed for 2 h at 450 °C to remove the residual mechanical stresses.

Ceramic samples of $(1-x)$PFB–(x)PbTiO$_3$ (PFB–xPT) have been obtained by solid-state reaction route using high-purity Fe_2O_3, Nb_2O_5, PbO, TiO_2 and Ta_2O_5. These oxides were batched in stoichiometric proportions, and 1 wt.% Li_2CO_3 was added to the batch. This addition promotes formation of the perovskite modifications of both PFN and PFT and reduces their conductivity [17–19]. After mixing thoroughly in an agate mortar under ethyl alcohol and subsequent drying, the green ceramic samples were pressed at 100 MPa in the form of disks of 10 mm in diameter and of 2–4 mm in height using polyvinyl alcohol as a binder. The sintering was performed at 1050–1150 °C for 2 h in a closed alumina crucible. The density of the obtained ceramics was about 90–95 % of the theoretical one. The electrodes for measurements were deposited to the grinded disks of 9 mm in diameter and of 0.9 mm in height by firing on silver past. Dielectric studies were carried out in the 10^2–10^6 Hz range in the course of both heating and cooling at a rate of 2–3 K/min with the aid of the computer-controlled E7-20 and Novocontrol Alpha-A impedancemeters. The piezoelectric coefficient, d_{31}, was measured using the standard resonance–antiresonance technique. The resonance and antiresonance frequencies were obtained using the maximum and minimum of admittance spectra. From these values, the d_{31} values were determined. Mössbauer spectra were measured with the aid of the MS-1104E rapid spectrometer of the latest design and analyzed using the original computer program UNIVEM. Magnetic measurements were performed using the PPMS-9 physical property measurement system (Quantum Design) in the temperature range 2–300 K and under magnetic field up to 90 kOe.

The X-ray diffraction study of the PFT powder was performed on a D8-ADVANCE diffractometer (Cu$K\alpha$ radiation, θ–2θ scan mode) using a VANTEC linear detector and a TTK 450 Anton Paar temperature chamber in the 130–300 K temperature range. The scan step in the angle 2θ was 0.016°. The unit cell parameters were determined and refined during fitting of the profiles using the WTREOR and DDM programs [20].

9.3 Results and Discussion

X-ray diffraction studies have shown that all the investigated compositions were single-phase and had a structure of the perovskite type. For PFT powder the unit cell parameters in all the temperature points in the 135–360 K range were obtained by fitting the X-ray diffraction profiles using the set of codes TOPAS 4.2 [19]. Some data necessary for fitting: space groups, orientation and the initial parameters of the Bravais cells as well as the coordinates of the atoms were taken from [4]. Thus obtained temperature dependence of the PFT unit cell parameters is

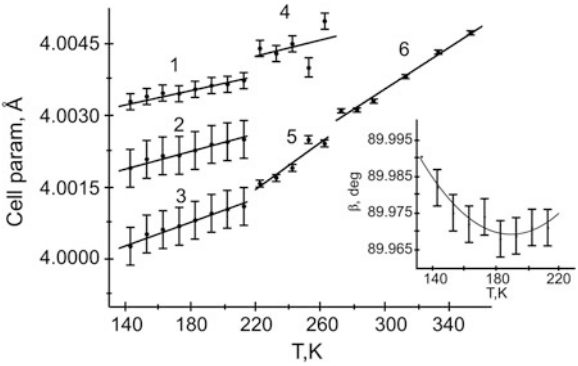

Fig. 9.1 Temperature dependences of the unit cell parameters for PFT powder in the monoclinic *Cm*, tetragonal *P4 mm* and cubic $Pm\bar{3}m$ phases: *1*—c_{mon}; *2*—$a_{mon}/\sqrt{2}$; *3*—$b_{mon}/\sqrt{2}$; *4*—c_{tetr}; *5*—a_{tetr}; *6*—a_{cub}. The inset shows temperature dependence of the monoclinic angle β

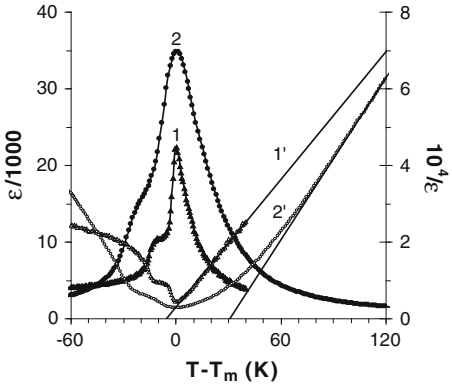

Fig. 9.2 Dependences of dielectric permittivity (1, 2) and reciprocal permittivity (1′, 2′) on the reduced temperature $T - T_m$ for PFN single crystal (1, 1′) and Li-doped PFN ceramics (2, 2′)

shown in Fig. 9.1. One can see the anomalies of the unit cell parameters at $T_{CT} \approx 270$ K and $T_{TM} \approx 220$ K. It should be mentioned that the monoclinic angle β shows unusual temperature dependence. At cooling its value at first remains nearly constant or even lowers, but below approximately 180 K it begins to increase and becomes close to 90° (see the inset in Fig. 9.2). This unusual behavior will be discussed in detail further.

Recently we have shown that, in contrast to a commonly adopted view, ferroelectric phase transition in PFN single crystals is non-diffused and usually observed in ceramic samples diffusion of the permittivity ε maximum has an extrinsic origin [7]. As one can see in Fig. 9.2 the $\varepsilon(T)$ anomalies corresponding to the monoclinic-tetragonal phase transition are well seen both in PFN single crystals and highly-resistive Li-doped PFN ceramics. However in ceramics, the extrapolated Curie–Weiss temperature T_{CW} is substantially higher than the temperature T_m of the $\varepsilon(T)$ maximum. Such behavior is typical of ferroelectrics with diffuse phase transition and may be induced in PFN ceramics by dopants (e.g. Li) and/or defects (e.g. lead and oxygen vacancies).

Figure 9.3 shows the temperature dependences of dielectric permittivity ε and loss tangent tan δ for highly-resistive Li-doped PFT ceramics measured at several

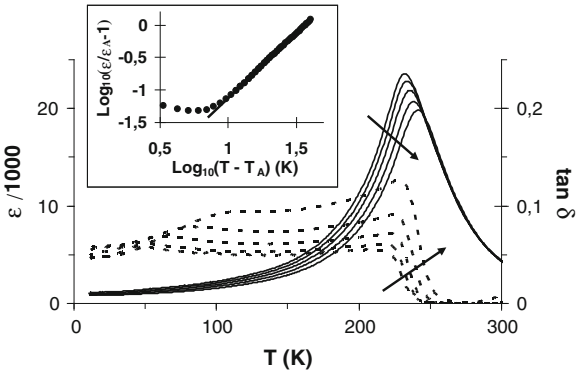

Fig. 9.3 Temperature dependences of permittivity (*solid lines*) and loss tangent (*broken lines*) measured at frequencies 10^2, 10^3, 10^4, 10^5 and 10^6 Hz for highly-resistive Li-doped PFT ceramics. The arrows show the direction of the frequency increase. The inset shows approximation of the high-temperature slope of the experimental $\varepsilon(T)$ peak (*points*) based on formula (9.2) (*straight line*)

frequencies. This ceramics exhibits a very large dielectric response and a pronounced frequency dispersion of both ε and tan δ. Temperature T_m of the $\varepsilon(T)$ maximum is similar to that reported in the literature for PFT ceramics and single crystals [3, 6, 21–23]. The T_m frequency shift, $\Delta T = T_m$ (10^6 Hz)–T_m (10^2 Hz) is much smaller than that for more conducting PFT single crystals [3], but is comparable with ΔT values reported for PFT ceramics studied in Refs. [21, 23]. The increase of T_m with the frequency is well fitted with the Vogel–Fulcher relation, typical of relaxors [24, 25]:

$$f = f_0 \exp[-E/k(T_m - T_0)] \tag{9.1}$$

where f_0 is the attempt frequency, E is the activation energy (the potential barrier height) and T_0 is the Vogel–Fulcher temperature, which is often associated with the freezing of relaxators and transition into the polar glass state. The Vogel–Fulcher freezing temperature $T_0 = 217$ K is close to the temperature of tetragonal-monoclinic phase transition. Other parameters of the Vogel–Fulcher relation for PFT ceramics, namely the attempt frequency $f_0 = 5 \cdot 10^{11}$ Hz and activation energy $E = 0.018$ eV, are very close to the ones reported for similar ternary perovskites $PbSc_{0.5}Ta_{0.5}O_3$ [24] and $PbSc_{0.5}Nb_{0.5}O_3$ [25] exhibiting spontaneous relaxor-ferroelectric transition.

At temperatures above T_m the $\varepsilon(T)$ of Li-doped PFT ceramics follows a quadratic law typical of relaxors and ferroelectrics with a diffuse phase transition [26]:

$$\frac{\varepsilon_A}{\varepsilon} = 1 + \frac{(T - T_A)^2}{2\delta^2} \tag{9.2}$$

with the parameters $T_A = 230$ K, $\varepsilon_A = 2.3 \cdot 10^4$ and $\delta = 26$ K. The value of the $\varepsilon(T)$ diffusion parameter δ for Li-doped PFT ceramics is somewhat larger than the

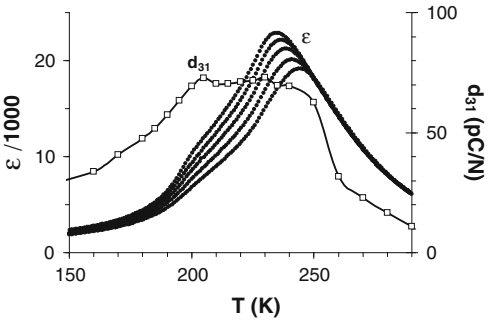

Fig. 9.4 Temperature dependences of piezoelectric modulus d_{31} and permittivity measured at frequencies 10^2, 10^3, 10^4, 10^5 and 10^6 Hz for poled Li-doped PFT ceramics in the zero field heating after field cooling ($E = 5$ kV/cm) mode

one for PFT single crystal ($\delta = 20$ K [26]). As one can see from Fig. 9.3, the $\varepsilon(T)$ maximum for PFT ceramics does not coincide with the $T_{CT} \approx 270$ K and there are no anomalies in the $\varepsilon(T)$ curve corresponding to $T_{TM} \approx 220$ K.

However after cooling under a bias field $E = 5$ kV from 250 K down to 50 K, there appears a step in the $\varepsilon(T)$ curve at about 200 K, its temperature does not depend on frequency (Fig. 9.4). It seems that this step corresponds to the tetragonal-monoclinic phase transition. This assumption is confirmed by the fact that temperature dependence of piezoelectric modulus exhibits a plateau in the 200–250 K range (Fig. 9.4) which approximately coincides with the range of the tetragonal phase determined from the structural studies (Fig. 9.1). Thus the tetragonal-monoclinic phase transition in PFN is not a spontaneous relaxor-ferroelectric transition, because the piezoelectric response does not disappear above T_{TM}. It seems that in the 220–270 K range both tetragonal and cubic phases coexist. This supposition explains the presence of diffuse frequency-dependent $\varepsilon(T)$ maximum between T_{TM} and T_{CT}.

For both PFN–xPT and PFT–xPT compositions T_m increases, as x grows (Fig. 9.5). The $\varepsilon(T)$ maximum diffusion does not change substantially with x for PFN–xPT ceramics [27]. In contrast to this for PFT–xPT compositions the $\varepsilon(T)$ maximum becomes sharper (Fig. 9.6) and its frequency shift ΔT diminishes (Fig. 9.5b). These results corroborate the data reported earlier for PFT–xPT system [28]. For all the PFT–xPT compositions studied, Curie–Weiss law is fulfilled at temperatures exceeding T_m by 40–50 K, but the extrapolated Curie–Weiss temperature T_{CW} appears to be substantially higher than T_m (Fig. 9.6). Similar behavior is observed for Li-doped PFN ceramics (Fig. 9.2). Addition of $PbTiO_3$ leads to decrease of the difference between T_{CW} and T_m. In PFN–xPT ceramics $T_{CW}(x)$ and $T_m(x)$ dependences converge at $x \approx 0.1$ and for compositions with $x > 0.1$ at larger x values $T_{CW} < T_m$ (Fig. 9.5a), as in usual ferroelectrics with a sharp phase transition. Thus Li-doped PFN–xPT ceramics with $x < 0.1$ and all the PFT–xPT ceramic compositions studied exhibit, from one side, the features typical of usual ferroelectrics (slightly diffused $\varepsilon(T)$ maximum, absence of the frequency shift of T_m, structural phase transition near T_m) and, from the other side, properties characteristic

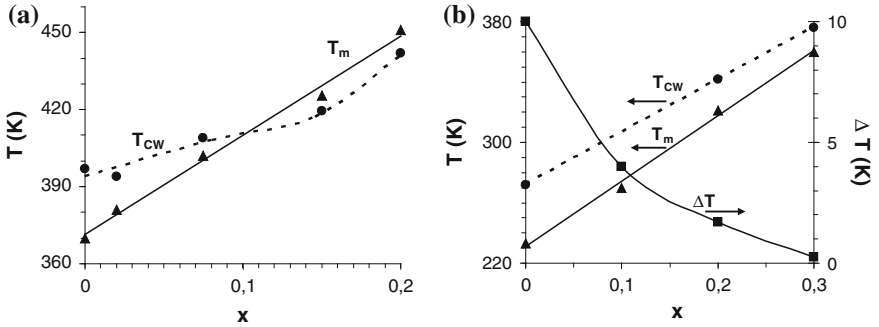

Fig. 9.5 Dependence of permittivity maximum temperature T_m, extrapolated Curie–Weiss temperature T_{CW} and T_m frequency shift ΔT on the composition for Li-doped PFN–xPT (**a**) and PFT–xPT (**b**) ceramics

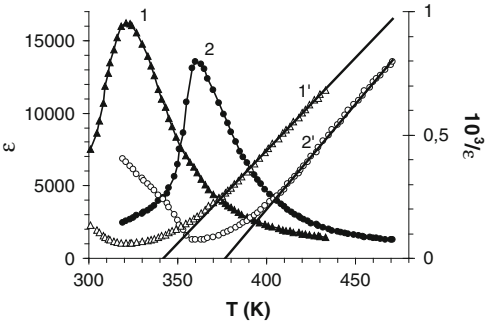

Fig. 9.6 Temperature dependences of permittivity (1, 2) and reciprocal permittivity (1′, 2′) measured at 1 kHz, for Li-doped PFT–0.2PT (1, 1′) and PFT–0.3PT (2, 2′) ceramics

of relaxors and ferroelectrics with diffuse phase transition (ε follows a quadratic law just above T_m, and the linear Curie–Weiss law is valid only at temperatures much higher than T_m with $T_{CW} > T_m$). Similar combination of contradictory properties was observed for $0.5PbMg_{1/3}Nb_{2/3}O_3$–$0.5PbTiO_3$ single crystals [29] where the structural phase transition takes place at T_m and neither conventional relaxor dispersion, nor the frequency shift of T_m are observed. Nevertheless, the universal relaxor dispersion still persists in these crystals and T_m corresponds no to the ferroelectric–paraelectric but rather to the ferroelectric-relaxor phase transition.

At room temperature Mössbauer ^{57}Fe spectra of all the compositions studied appeared to be doublets with quadrupole splitting of $\approx$0.4 mm/s and isomer shift of $\approx$0.4 mm/s (relative to metallic iron), corresponding to the Fe^{3+} ions occupying the octahedral sites of perovskite lattice. This result is in a good agreement with the data of the X-ray photoelectron studies showing for PFN single crystals and ceramics the presence of only trivalent iron within the sensitivity of the method [30]. When cooling below the Neél temperature, T_N, the Mössbauer spectrum transforms from doublet to sextet [7, 14, 21, 31]. This transformation is accompanied by a dramatic decrease of the magnitude η of doublet intensity normalized to its value at 300 K (Fig. 9.7). This abrupt drop in the temperature dependence of

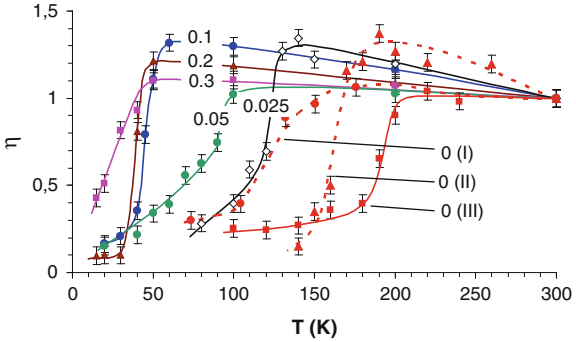

Fig. 9.7 Temperature dependences of η-maximal intensity of the doublet in Mössbauer spectrum related to its value at 300 K for some Li-doped PFT–xPT compositions. Numbers at the curves correspond to x values; 0(I) and 0(II)—Li-doped PFT ceramics sintered at different temperatures [21]; 0(III)—PFT powder, used for X-ray studies

η allows one to obtain T_N from the Mössbauer experiment. This method was successfully used previously to determine values of T_N in several multiferroics and their solid solutions and the results obtained were very similar to the data obtained by traditional methods such as the magnetization or magnetic susceptibility measurements (see [21, 31] and references therein). Li-doping is known to stimulate the compositional ordering in ternary $PbB^{3+}_{0.5}Nb_{0.5}O_3$ perovskites [32]. Such ordering may decrease dramatically the T_N values due to reducing the number of the neighboring magnetic Fe^{3+} ions around the given Fe^{3+} ion. Indeed, Li-doped PFT ceramics, exhibit a large scatter of T_N values, depending on the sintering temperature (curves 0(I) and 0(II) in Fig. 9.7). This scatter can also originate from the changes in the degree of Fe clustering in the lattice [14]. Ceramics sintered at high enough temperature, usually have $T_N \approx$ 160–170 K which corresponds well to the majority of the data published for PFT [6, 22]. The largest $T_N \approx$ 180–190 K was observed for PFT powder (curve 0(III) in Fig. 9.7) used for X-ray studies. It is worth noting this T_N value coincides well with the temperature at which the minimum in the $\beta(T)$ dependence is observed for the same PFT powder (inset in Fig. 9.1). At the same temperature one can see some small anomalies in the temperature dependence of the monoclinic unit cell parameters (Fig. 9.1, curves 1–3), however these anomalies are within the experimental error. It seems that the minimum in the $\beta(T)$ dependence and tiny anomalies of unit cell parameters are due to the magnetoelastic coupling which is believed to maximize in the vicinity of T_N. Note, that anomalies in the temperature dependence of the unit cell parameters in the vicinity of T_N have been already observed in PFN ceramics [33].

There are a lot of literature data on the temperature dependences of magnetization (M) for PFN and PFT single crystals and ceramics [1, 6, 8, 10, 11, 22]. These dependences were also reported for PFN–xPT single crystals [8] and ceramics [11] in the composition range $0 \leq x \leq 0.2$ and $0 \leq x \leq 0.15$, respectively. In the present work we studied the $M(T)$ dependences for Li-doped PFT–xPT ceramics

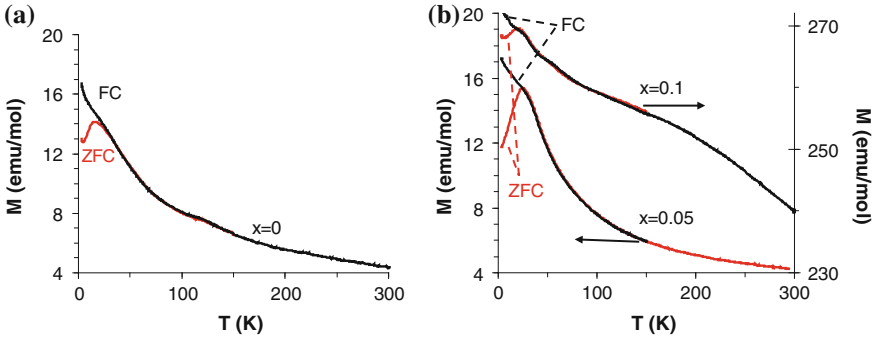

Fig. 9.8 Temperature dependences of magnetization M measured under a magnetic field of 1 kOe in the ZFC and FC modes for Li-doped PFT–xPT ceramics: **a** $x = 0$; **b** $x = 0.05$ and $x = 0.1$

(Fig. 9.8). For this ceramics, the $M(T)$ dependence is very similar to the one observed for PFN and PFT single crystals: during heating under a magnetic field of 1 kOe after zero field cooling (ZFC) it has a maximum at 16 K (Fig. 9.8a). Besides this maximum there is also a bump on the $M(T)$ curve at about 130 K corresponding to AFM–PM transition. As was already mentioned above, the T_N values of Li-doped PFT ceramics are often lower than those of undoped ceramics and single crystals due to possible partial ordering or/and a change in the degree of Fe-ions clustering. The $M(T)$ dependence measured in the field-cooled (FC) mode nicely coincides with the one measured in the ZFC mode except a low-temperature region where the FC curve does not show a maximum. Such a difference between the $M(T)$ curves measured in the ZFC and FC modes is typical of a spin-glass state [2, 8]. For compositions with $x \geq 0.05$ only the low-temperature maximum is observed in the $M(T)$ curves measured in the ZFC mode (Fig. 9.8b). This is typical of solid solutions of multiferroics, where a small bump corresponding to T_N duffuses and finally disappears on increasing the concentration of the nonmagnetic component [8, 11]. For example in the PFN–xPT ceramics a bump corresponding to T_N is observed only for compositions with $x \leq 0.04$ [11]. However the anomalies of the doublet intensity in the Mössbauer spectrum are well seen for all the PFN–xPT and PFT–xPT compositions studied (Fig. 9.7). One of the samples ($x = 0.1$) exhibited unusually high M values which were more than an order of magnitude larger as compared to the other compositions studied. Both the ZFC and FC $M(T)$ curves of this sample were much more diffused than the ones for the other samples studied. Moreover the PFT–0.1PT sample exhibited the well-defined magnetic hysteresis $M(H)$ loops even at room temperature. It is worth noting that very similar M values as well as $M(T)$ and $M(H)$ dependences were reported recently for PFT ceramic sample studied in [6]. We suppose that such unusual behavior is due to the presence in the PFT–xPT sample with $x = 0.1$ a small quantity of ferromagnetic impurity, presumably $PbFe_{12}O_{19}$.

In the PFT–xPT compositions studied, the temperature T_g of the $M(T)$ maximum at first increases with x but at larger x values begins to decrease (Fig. 9.9). It

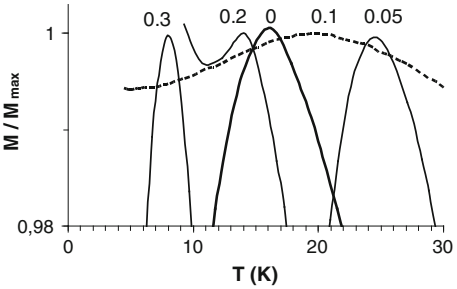

Fig. 9.9 Temperature dependences of magnetization M normalized to its maximal value M_{max} for Li-doped PFT–xPT ceramics. Measurements were carried out under a magnetic field of 1 kOe in the ZFC mode. Numbers at the curves correspond to x values

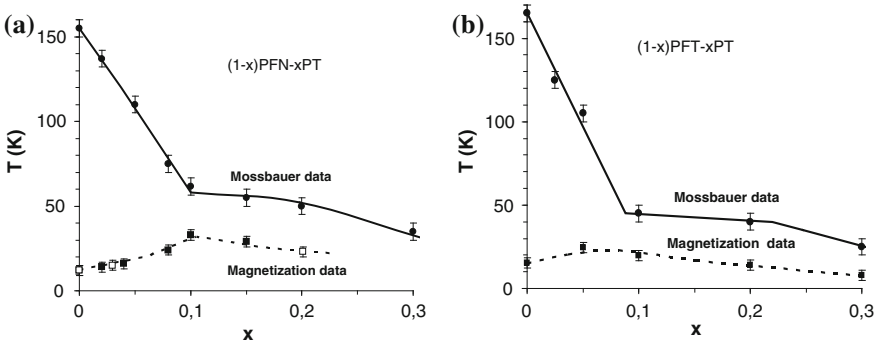

Fig. 9.10 Compositional dependences of the temperatures of $\eta(T)$ anomaly (*filled circles*, *solid lines*) and the maximum of the $M(T)$ dependence in the ZFC mode (*squares*, *broken lines*) for PFN–xPT and PFT–xPT ceramics. Magnetization data for PFN–xPT are plotted using the data of [11] for ceramics (*filled squares*) and [8] for single crystals (*open squares*)

is worth noting that a similar increase of T_g was observed previously in the PFN–xPT ceramics in the $x < 0.1$ compositional range [11]. This increase was attributed to a slight decrease of the lattice parameter with x and a subsequent increase of the magnetic coupling. However the similar character of the $T_g(x)$ dependence was observed in the PFN–xBaFN solid solution system, where the lattice parameter increases with x [8]. We suppose that the observed increase of T_g in both PFN–xPT and PFT–xPT solid solution systems is a result of the increase of the average size of the confined percolation clusters, with x, because of the decrease of strength of the infinite cluster [8].

The results of Mössbauer and magnetization studies for both PFN–xPT and PFT–xPT solid solution systems are summarized in Fig. 9.10. According to Mössbauer data at $x < 0.1$, T_N rapidly decreases as x grows. Lowering of T_N with x in both systems is quite expectable due to dilution of the magnetic subsystem. However above a certain compositional threshold ($x \approx 0.1$) fast lowering of T_N with the increase of the Ti concentration stops and a new magnetic state with

comparatively high ($\sim$50 K) transition temperature becomes stable in a rather wide compositional range (Fig. 9.10). According to magnetization data, in this compositional range ($x > 0.1$) the magnetic state is a spin-glass-like. In both PFN–xPT and PFT–xPT systems, the T_g values are lower by about 20 K than the temperatures of magnetic phase transition determined from the Mössbauer studies. This difference seems to be caused by the fact that the upper limit of the spin relaxation rates in these samples is above the characteristic Mössbauer time [34]. Similar behavior was reported e.g. for $PbFe_{12-x}Cr_xO_{19}$ hexaferrites [35].

9.4 Summary

In summary, highly-resistive Li-doped $(1-x)PbFe_{0.5}B_{0.5}O_3$–$(x)PbTiO_3$ (B = Nb, Ta) ceramics were obtained by conventional sintering with high density and pure perovskite phase. Dielectric, X-ray, Mössbauer and magnetization studies of ceramics with the $0 < x < 0.3$ composition range have been carried out. Addition of $PbTiO_3$ to $PbFe_{0.5}B_{0.5}O_3$ increases the temperature T_m of the permittivity maximum, decreases the diffusion of this maximum and lowers the Neél temperature T_N. However above a certain compositional threshold ($x \approx 0.1$) fast lowering of T_N stops and a new magnetic state stable in a rather wide compositional range appears. Large difference between the zero-field cooled and field-cooled magnetization curves as well as between the temperatures of magnetic phase transition determined from Mössbauer and magnetization studies for compositions with $x > 0.1$ implies that this state is a spin glass phase.

We suppose that both the maximum of the $T_g(x)$ dependence and a sharp change of the slope of $T_N(x)$ dependence at $x \approx 0.1$ are the fingerprints of a percolation phase transition in the $(1-x)PbFe_{0.5}B_{0.5}O_3$–$(x)PbTiO_3$ solid solution systems. As soon as such a (geometrical) phase transition is a critical phenomenon, one may expect an enhancement of all physical responses in the crystal matrix, and, in particular, the enhancement of the magnetoelectric response.

Acknowledgments This work was partially supported by the Russian Foundation for Basic Research (RFBR) project # 12-08-00887_a, and the Research Committee of the University of Macau under Research & Development Grant for Chair Professor.

References

1. V.A. Bokov, I.E. Mylnikova, G.A. Smolenskii, Sov. Phys. JETP. **15**, 447 (1962)
2. W. Kleemann, V.V. Shvartsman, P. Borisov, A. Kania, Phys. Rev. Lett. **105**, 257202 (2010)
3. I.P. Raevskii, V.V. Eremkin, V.G. Smotrakov, M.A. Malitskaya, S.A. Bogatina, L.A. Shilkina, Kristallogr. Rep. **47**, 1007 (2002)
4. N. Lampis, P. Sciau, A.G. Lehmann, J. Phys.: Condens. Matter **12**, 2367 (2000)
5. N. Lampis, C. Franchini, G. Satta, A. Geddo-Lehmann, S. Massidda, Phys. Rev. B **69**, 064412 (2004)

6. R. Martinez, R. Palai, H. Huhtinen, J. Liu, J.F. Scott, R.S. Katiyar, Phys. Rev. B **82**, 134104 (2010)
7. I.P. Raevski, S.P. Kubrin, S.I. Raevskaya, S.A. Prosandeev, M.A. Malitskaya, V.V. Titov, D.A. Sarychev, A.V. Blazhevich, I.N. Zakharchenko, IEEE Trans. Ultrason. Ferroelect. Freq. Contr. **59**, 1872 (2012)
8. V.V. Laguta, M.D. Glinchuk, M. Marysko, R.O. Kuzian, S.A. Prosandeev, S.I. Raevskaya, V.G. Smotrakov, V.V. Eremkin, I.P. Raevski, Phys. Rev. B **87**, 064403 (2013)
9. D.A. Sanchez, N. Ortega, A. Kumar, G. Sreenivasulu, R.S. Katiyar, J.F. Scott, D.M. Evans, M. Arredondo-Arechavala, A. Schilling, J.M. Gregg, J. Appl. Phys. **113**, 074105 (2013)
10. A. Falqui, N. Lampis, A. Geddo-Lehmann, G. Pinna, J. Phys. Chem. B **109**, 22967 (2005)
11. S.P. Singh, S.M. Yusuf, S. Yoon, S. Baik, N. Shin, D. Pandey, Acta Mater. **58**, 5381 (2010)
12. G.-M. Rotaru, B. Roessli, A. Amato, S.N. Gvasaliya, C. Mudry, S.G. Lushnikov, T.A. Shaplygina, Phys. Rev. B **79**, 184430 (2009)
13. H. Schmid, Ferroelectrics **162**, 317 (1994)
14. I.P. Raevski, S.P. Kubrin, S.I. Raevskaya, D.A. Sarychev, S.A. Prosandeev, M.A. Malitskaya, Phys. Rev. B **85**, 224412 (2012)
15. V.V. Laguta, J. Rosa, L. Jastrabik, R. Blinc, P. Cevc, B. Zalar, M. Remskar, S.I. Raevskaya, I.P. Raevski, Mater. Res. Bull. **45**, 1720 (2010)
16. V.M. Yudin, A.G. Tutov, A.B. Sherman, V.A. Isupov, Izv. Akad. Nauk SSSR Ser. Fiz. **31**(11), 1798 (1967) (In Russian)
17. I.P. Raevskii, S.T. Kirillov, M.A. Malitskaya, V.P. Filippenko, S.M. Zaitsev, L.G. Kolomin, Izv. AN SSSR. Neorg. Mater. **24**, 286 (1988) (In Russian) [English translation: Inorg. Mater. **24**, 217 (1988)]
18. V.Y. Shonov, I.P. Raevski, A.A. Bokov, Zhurnal Tekhnicheskoi Fiziki. **66**, 98 (1996) (In Russian) [English translation: Tech Phys. **41**, 166 (1996)]
19. I.P. Raevski, S.P. Kubrin, S.A. Kovrigina, S.I. Raevskaya, V.V. Titov, A.S. Emelyanov, M.A. Malitskaya, I.N. Zakharchenko, Ferroelectrics **397**, 96 (2010)
20. Bruker AXS TOPAS V4, *General Profile and Structure Analysis Software for Powder Diffraction Data* (User's Manual, Bruker AXS, Karlsruhe, Germany, 2008)
21. I.P. Raevski, S. Kubrin, S.I. Raevskaya, V.V. Stashenko, D.A. Sarychev, M.A. Malitskaya, M.A. Seredkina, V.G. Smotrakov, I.N. Zakharchenko, V.V. Eremkin, Ferroelectrics **373**, 121 (2008)
22. S. Nomura, H. Takabayashi, T. Nakagawa, Jpn. J. Appl. Phys. **7**, 600 (1968)
23. W.Z. Zhu, A. Kholkin, P.Q. Mantas, J.L. Baptista, J. Eur. Ceram. Soc. **20**, 2029 (2000)
24. F. Chu, N. Setter, A.K. Tagantsev, J. Appl. Phys. **74**, 5129 (1993)
25. I.P. Raevski, V.V. Eremkin, V.G. Smotrakov, E.S. Gagarina, M.A. Malitskaya, Fizika Tverd. Tela. **42**, 154 (2000) (In Russian) [English translation: Phys. Solid State **42**, 161 (2000)]
26. A.A. Bokov, Y.-H. Bing, W. Chen, Z.-G. Ye, S.A. Bogatina, I.P. Raevski, S.I. Raevskaya, E.V. Sahkar, Phys. Rev. B **68**, 052102 (2003)
27. E.I. Sitalo, I.P. Raevski, A.G. Lutokhin, A.V. Blazhevich, S.P. Kubrin, S.I. Raevskaya, Y.N. Zakharov, M.A. Malitskaya, V.V. Titov, I.N. Zakharchenko, IEEE Trans. Ultrason. Ferroelect. Freq. Contr. **58**, 1914 (2011)
28. S.Y. Cho, J.S. Kim, M.S. Jang, J. Electroceram. **16**, 369 (2006)
29. A.A. Bokov, H. Luo, Z.-G. Ye, Mater. Sci. Engin. B **120**, 206 (2005)
30. A.T. Kozakov, A.G. Kochur, K.A. Googlev, A.V. Nikolsky, I.P. Raevski, V.G. Smotrakov, V.V. Yeremkin, J. Electron Spectrosc. Relat. Phenom. **184**, 16 (2011)
31. I.P. Raevski, S.P. Kubrin, S.I. Raevskaya, V.V. Titov, D.A. Sarychev, M.A. Malitskaya, I.N. Zakharchenko, S.A. Prosandeev, Phys. Rev. B **80**, 024108 (2009)
32. A.A. Bokov, V.Y. Shonov, I.P. Rayevsky, E.S. Gagarina, M.F. Kupriyanov, J. Phys. Condens. Matter. **5**, 5491 (1993)
33. S.P. Singh, D. Pandey, S. Yoon, S. Baik, N. Shin, Appl. Phys. Lett. **90**, 242915 (2007)
34. I.A. Campbell, Hyperfine Interact. **27**, 15 (1986)
35. G. Albanese, B.E. Watts, F. Leccabue, S. Diaz Castanon, J. Magn. Magn. Mater. **184**, 337 (1998)